Mechanical and functional properties of ultrafine grained Al wires reinforced by nano-Al_2O_3 particles

R. Casati [a,*], X. Wei [b], K. Xia [b], D. Dellasega [c], A. Tuissi [d], E. Villa [d], M. Vedani [a]

[a] Department of Mechanical Engineering, Politecnico di Milano, Via La Masa 1, 20156 Milano, Italy
[b] Department of Mechanical Engineering, University of Melbourne, Victoria 3010, Australia
[c] Department of Energy, Politecnico di Milano, Via Ponzio 34, 20133 Milano, Italy
[d] CNR-IENI, Corso Promessi Sposi 29, 23900 Lecco, Italy

Received 29 April 2014
Accepted 24 July 2014
Available online 4 August 2014

1. Introduction

Metal matrix nanocomposites (MMnCs) are considered interesting materials since they show higher strength than the corresponding base metals while retaining a good toughness [1–3]. They are generally made up of a ductile metal matrix reinforced with hard nanoparticles (NPs). Different from precipitates formed in precipitation hardening alloys, the reinforcing NPs are thermodynamically stable, making MMnCs ideal for high temperature applications [1–3]. Such small particles can obstruct the motion of dislocations and are responsible for the formation of geometrically necessary dislocations due to the mismatch in coefficients of thermal expansion and in elastic moduli between the metal matrix and the NPs [4]. Low wettability and a high surface to volume ratio of ceramic nano-particles are the main issue to face to prepare MMnCs. NPs tend to agglomerate and form clusters, losing their capability to effectively obstruct the movement of dislocations. For this reason, they cannot be prepared by conventional casting methods. To overcome this problem several non-conventional manufacturing methods have been proposed, and they can be categorized into two major groups: ex-situ and in-situ synthesis routes [1–3]. The former refers to those processes in which the nano-reinforcement is added to the liquid or powder metal whereas the latter refers to those methods that lead to the formation of nano-sized compounds during the process itself, e.g. through reacting gases. Powder metallurgy routes [5–10], ultrasound assisted casting [11,12], disintegrated melt deposition [13] are some of the processes commonly used to produce MMnCs.

The high strength of MMnCs can be further improved by decreasing the grain size of the matrix down to the sub-micrometer level (Hall–Petch strengthening) [14]. Indeed, ultrafine grained (UFG) materials, processed by severe plastic deformation methods like equal channel angular pressing or high pressure torsion, have attracted growing interest because of their unique physical and mechanical properties [15]. The combination of properties conferred to the aluminum matrix by the combination of an UFG microstructure and hard NPs would be particularly attractive for all those applications requiring low density and high mechanical properties.

In this investigation, a powder metallurgy route to produce Al-based MMnCs reinforced by Al_2O_3 NPs is adopted. An UFG microstructure was conferred to the micro Al particles through high-energy ball milling (BM) and preserved during consolidation thanks to the oxide dispersion. Ball milling has proven to be a suitable technique for breaking the surface oxide layer that covers the aluminum particles into nano-sized fragments (in-situ production of NPs). It also revealed able to embed NPs into the ductile Al matrix. The ball milled powder, after canning, were consolidated via hot extrusion. The extruded rods were cold rolled down into

* Corresponding author. Tel.: +39 02 2399 8638.
E-mail address: riccardo.casati@polimi.it (R. Casati).

wires to verify the formability. The wires were then characterized for mechanical properties (tensile and Vickers hardness) and microstructures including NPs dispersion and grain sizes by electron microscopy analysis.

The damping capacity, or internal friction (IF), was also investigated. IF is a measure of the energy dissipated by a material during imposed mechanical vibration under cyclic loading. IF of the Al/Al_2O_3 MMnC wires was studied to consider these materials as possible candidates for applications in which the combination of good mechanical properties and high internal friction required. Indeed, vibrations generated in response to a dynamic loading are responsible for high noise levels, premature fatigue failure and wear in most of the frequently used structural materials such as steels and Al alloys which exhibit relatively low IF [16,17].

2. Method

A commercial purity Al powder with an average size of 20 μm (supplied by ECKA Granules) and a colloidal solution of alumina particles with an average particle size of 50 nm in isopropyl alcohol (supplied by Sigma Aldrich) were used as starting materials. The aluminum particles were passivated by exposure to air to possess a thin oxide layer. According to previous works [18–23], the thickness of this layer is considered to be in the range of 2–4 nm. The nominal oxygen content in the Al powder was <0.5 wt.% (data supplied by ECKA Granules). A scheme of the starting materials used for MMnCs manufacturing is depicted in Fig. 1.

The Al powder was added to the colloidal solution (with 2 wt.% of ex-situ Al_2O_3 NPs in the composite) and the mixture was stirred in a beaker and then dried at 50 °C. After this operation, the Al particles were covered by the NPs in clusters, as illustrated in Fig. 2.

High energy ball milling was performed on the Al powder or the Al–2 wt.% Al_2O_3 powder by using a Vario-Planetary Mill Pulverisette 4 equipped with steel vials and balls (10 mm in diameter). 1.5 vol.% of ethanol was used as process control agent to avoid excessive cold welding and agglomeration of the particles. To minimize oxidation during attrition, the two vials were back-filled with argon. The milling was performed for 16 h with a ball-to-powder weight ratio of 10:1. An excessive temperature rise was avoided by interrupting the procedure for 10 min after each 30 min of milling. The speed of the main disk was set at 250 rpm clockwise whereas the speed of the two planets at 200 rpm counter-clockwise. After milling, the powders were packed in cylindrical Cu alloy cans (external diameter = 10 mm and thickness = 1 mm). They were closed by means of press-fit plugs and then subjected to hot extrusion at 400 °C, as described in [24]. The extrusion speed was 5 mm/min. The die was heated by an induction coil and the temperature was monitored by a type-K thermocouple. The starting billet diameter was reduced to 4 mm after extrusion. After hot deformation, the can material was stripped off and the rods were cold rolled down to a square section of 1 mm^2 by a caliber rolling mill, with intermediate annealing at 400 °C for 5 min after each area reduction of about 20%.

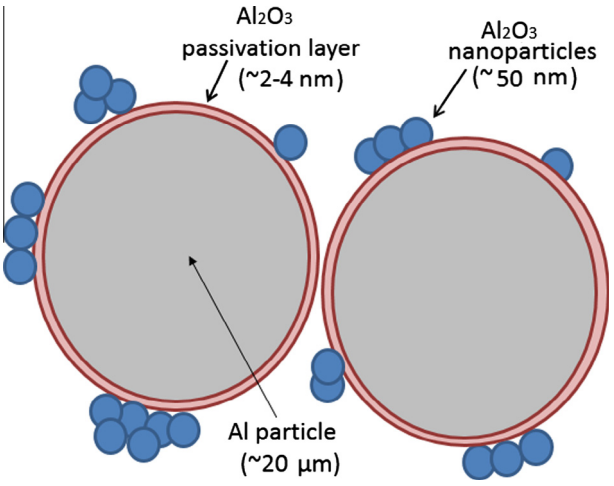

Fig. 2. Schematic of Al particles covered by alumina NPs after mixing and drying.

The density of the materials was estimated based on the Archimedes' principle using polished samples. Five measurement were performed for each type of sample.

Microstructural analysis of the transversal section of the rolled wires was carried out by scanning electron microscopy (SEM) – Zeiss Supra 40 equipped with a high efficiency in-lens SE detector. To obtain better contrast between the NPs and matrix, samples were etched with the Keller's solution. TEM foils with a final thickness of ~100 nm were prepared using a Nova Nanolab 200 focused ion beam (FIB). High angle annular dark field (HAADF) imaging by scanning transmission electron microscopy (STEM) was performed using a FEI Tecnai F20 operating at 200 kV. X-ray diffraction (XRD) was performed using PANalitical X-Pert PRO equipped with a RTMS X'Celerator sensor. Cu Kα (λ = 0.15418 nm) radiation was used. The crystallite size and micro-strain were calculated using the Williamson–Hall analysis [25].

Vickers microhardness (HV) was measured using Future Tech Corp. FM-700, applying a 2 N load for 15 s. The gauge length of the samples was 30 mm and the cross-section was 1 mm^2. Tensile tests were performed with a crosshead speed of 0.5 mm/min ($d\varepsilon/dt = 2.7 \times 10^{-4}\ s^{-1}$). Since the wire samples were too short to adopt special clamps for wires, premature fractures occasionally occurred close to the clamping position at strain levels exceeding about 4.5%. For this reason, the stress–strain curves presented have been are terminated at a strain of 4.5%.

Mechanical spectroscopy [26] is a technique that consists of applying a sinusoidal stress to a material and measuring the strain response. IF is related to the time-dependent elasticity of a material. Metals and alloys respond to an applied load not only by time-independent elastic strain, but also by time-dependent strain that lags behind the applied load. Because of the lag induced by the relaxation, the stress σ and strain ε can be expressed as:

$$\sigma = \sigma_0 \exp(i\omega t) \quad (1)$$

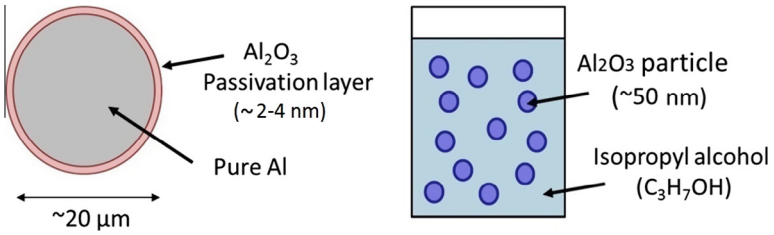

Fig. 1. Schematics of a passivated aluminum particle and the colloidal solution of alumina particles in isopropyl alcohol.

$$\varepsilon = \varepsilon_0 \exp(i\omega t - \delta) \tag{2}$$

where σ_0 and ε_0 are the stress and strain amplitudes, respectively, ω is the angular vibration frequency and δ is the loss angle by which the strain lags behind the stress. By combining these two equations, the resultant complex modulus, E is defined as:

$$E = \frac{\sigma_0}{\varepsilon_0}(\cos\delta + i\sin\delta) = E' + iE'' \tag{3}$$

where E' is the storage modulus and E'' the loss modulus. The storage modulus represents the stiffness whereas the loss modulus is a measure of the oscillation energy transformed into heat. The ratio of the loss modulus to the storage modulus is usually defined as $\tan\delta$ and commonly used to indicate the damping capacity of a material:

$$\tan\delta = \frac{E''}{E'} \tag{4}$$

Accordingly, the IF results in the present investigation are expressed in terms of $\tan\delta$ as a function of temperature. The tests were carried out using a DMA Q800 TA Instrument equipped with a liquid nitrogen cooling system. The samples were tested in the single cantilever configuration at 0.1, 1 and 10 Hz in the temperature range of −130 to 400 °C with a heating rate of 2 °C/min. The width (1 mm) and the thickness (1 mm) of the wire were measured by micrometer (±0.01 mm). The length of the specimens was 17.5 mm.

3. Results and discussion

3.1. Microstructures

Morphological analysis of powders was carried out before and after milling which was responsible for severe alteration of the shape of metal particles. The as-received Al particles were round, smooth and separated but, after ball milling, they appeared agglomerated and became flat with sharp corners (Fig. 3). The Al–2 wt.% Al_2O_3 powder had a similar appearance after milling. In Fig. 4a, a close-up of the milled particles. It is reasonable to assume that high-energy ball milling was able to break the alumina particle clusters and fragmentize the surface oxide into small pieces, forming in-situ alumina particles (Fig. 4b). Thus, high-energy ball milling may lead to two types of nanocomposites:

(a) the Al powder milled alone to produce MMnCs reinforced with oxide particles formed by fragmentation of the surface oxide layers, i.e. produced in-situ; and
(b) the Al–2 wt.% Al_2O_3 powder milled to produce MMnCs reinforced by a combination of alumina particles produced in-situ and alumina particles added ex-situ.

The milling process led to severe plastic deformation of the particles. The effect was evaluated by XRD technique. Peak broadening and a reduction in peak intensity were observed after milling for both the Al and Al–2 wt.% Al_2O_3 composite powders. Peak broadening is due to micro-strain caused by lattice defects and to reduction in the crystallite size. The crystallite size and micro-strain was estimated by Williamson–Hall method and the results are summarized in Table 1. The average crystallite size of the as-received Al powder was estimated to be 662 nm and the micro-strain 0.03%. The effect of ball milling (BM) was similar on the Al and composite powders. It led to a significant reduction in the crystallite size to about 120 and 114 nm, respectively, and to an increase in the micro-strain to 0.17%.

After ball milling, the powders were successfully consolidated through hot extrusion and then cold rolled without failures down to square wires (1 mm × 1 mm). The square section was constant along the length of the wires, which was about 30 cm. The whole process aimed at obtaining fully dense composite materials with in-situ and ex-situ Al_2O_3 particles embedded into Al particles during milling and well dispersed in the metal matrix after extrusion.

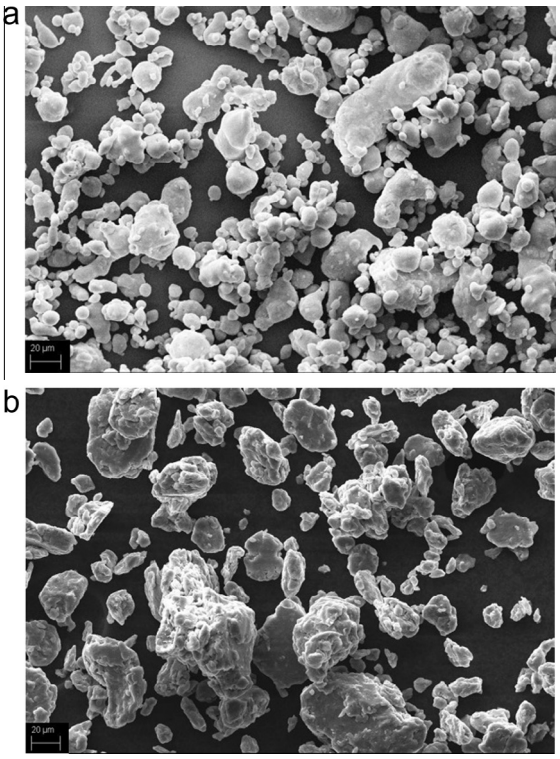

Fig. 3. (a) As-received Al powder and (b) the Al powder after 16 h of high-energy ball milling.

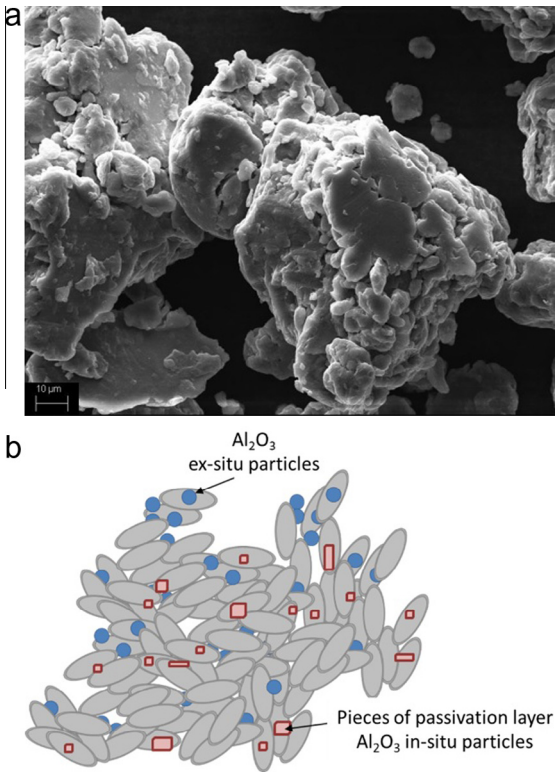

Fig. 4. (a) Clusters of the milled Al particles and (b) schematic of what might have happened during milling.

Table 1
Crystallite size and micro-strain of the powders and wires obtained from XRD results by the Williamson–Hall analysis.

	Crystallite size (nm)	Micro strain (%)
Al powder as-received + Al_2O_3 passivation layer	662	0.03
Al powder + in-situ Al_2O_3 particles after BM	120	0.17
Al powder + in-situ Al_2O_3 particles + 2% wt. ex-situ Al_2O_3 particles after BM	114	0.17
Al wire + in-situ Al_2O_3 particles	228	0.10
Al wire + in-situ Al_2O_3 particles + 2%wt. ex-situ Al_2O_3	206	0.12

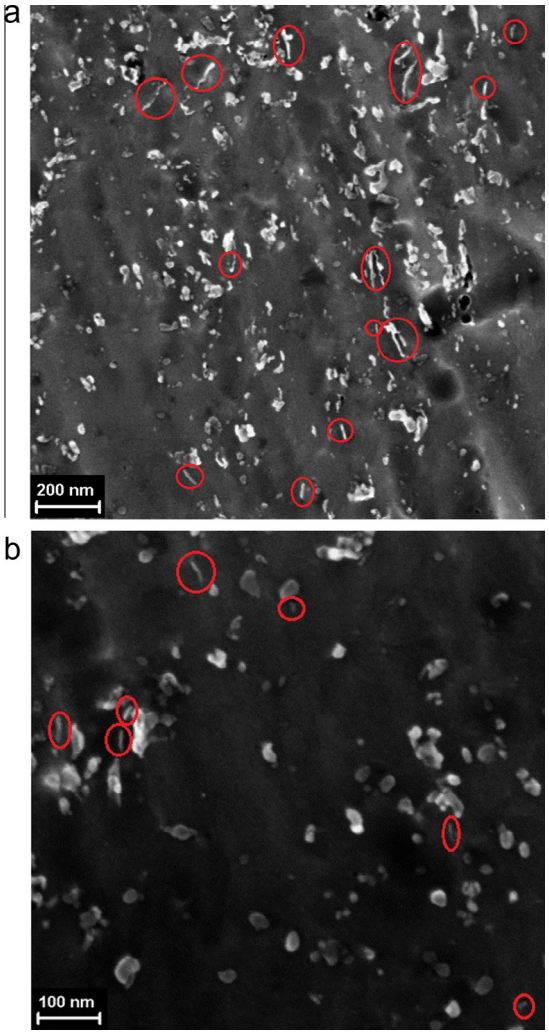

Fig. 5. SEM micrographs of the Al sample reinforced with the in-situ Al_2O_3 NPs at (a) low and (b) high magnifications.

The average density of the wires was (2.708 ± 0.008) g/cm^3 and (2.716 ± 0.008) g/cm^3, respectively.

The particle dispersion in the MMnCs wires was evaluated by SEM and TEM. In Fig. 5, the microstructure of the Al sample after etching is presented. As expected, the BM process led to the breaking into small fragments of the surface oxide layers. It is worth noting that these particles formed in-situ, revealed to be nano-sized and homogeneously distributed in the Al matrix. The oxide particles were generally smaller than 50 nm. The fragments aligned to the rolling direction (highlighted with red[1] circles in Fig. 5) seem to confirm the thickness of the passivation layer measured in previous research work (<4 nm) [18–23]. The particle size and distribution were also investigated by TEM-EDX chemical mapping (Fig. 6). The particles are outlined by the oxygen-rich areas and their sizes were consistent with those from SEM. Owing to their small sizes, these NPs are expected to act as obstacles for dislocation slip (Orowan strengthening) when they are not placed at grain boundaries [27].

Fig. 7 represents the microstructure of the composite wire reinforced with in-situ Al_2O_3 as well as 2 wt.% ex-situ Al_2O_3 NPs. The fraction of oxide is of course higher and some small clusters are also present. It is worth noting that the micrographs shown in Figs. 5 and 7 were from etched specimens. Therefore, the actual amount of the reinforcement oxide should be lower than it seems. The chemical etching, indeed, removed part of the Al matrix from the surface of the samples, leaving a higher fraction of nanoparticles. For the sake of clearness, the schematic depicted Fig. 8 describes in a simplified form the whole consolidation process. In Fig. 9, the HAADF images highlight the grain structures in the two types of wires, both showing ultrafine grains. The average grain size of the Al wire reinforced with 2 wt.% of ex-situ Al_2O_3 NPs was slightly smaller than that of the Al wire reinforced only with the in-situ NPs (180 nm and 220 nm respectively, as measured by the linear intercept method).

Although the samples were extruded and annealed at a high temperature (400 °C), it can be assumed that grain growth was restricted by NPs which possibly acted as pinning points on grain boundaries. The crystallite size of the wires calculated showed that the growth of the coherently scattering domains was limited (Table 1). For the Al wire reinforced with the in-situ particles the grain size was estimated to be 228 nm (120 nm before extrusion) and for the wire reinforced also with the ex-situ particles, the grain size was 206 nm (114 nm before extrusion), in fairly good agreement with the results from TEM. The results summarized in Table 1 also show that the micro-strain decreased only slightly, even though the consolidation and annealing were performed at 400 °C. It means that a high amount of lattice defects is retained in the matrix.

3.2. Mechanical properties

Vickers hardness tests and tensile tests were carried out in order to estimate the mechanical properties of the wires. The Al wire reinforced with the ex-situ particles showed higher hardness than the wire only reinforced with the in-situ particles (106 ± 1 HV vs. 96 ± 1 HV). These values are considerably higher than those typically found in commercial purity (CP) Al (~20 HV) and in UFG CP Al (~40 HV) [28]. The tensile results are summarized in Table 2 and typical tensile stress–strain curves are shown in Fig. 10. The wire reinforced ex-situ also showed both higher yield strength (YS) and ultimate tensile strength (UTS). Therefore, MMnCs showed YS and UTS values much higher than those generally related to pure Al [29]. In particular, the material reinforced with 2 wt.% of ex-situ Al_2O_3 reached YS and UTS of 282 MPa and 373 MPa while the composite reinforced with in-situ Al_2O_3 reached YS and UTS of 225 MPa and 302 MPa, respectively. By comparison, CP Al and UFG CP Al show much lower YS of 20 MPa and 110 MPa and UTS of 30 MPa and 120 MPa, respectively [24]. The improvement is possibly due to the additive strengthening effects of dispersed nanoparticles, ultrafine grain sizes and coefficient of thermal expansion (CTE) mismatch that generates increased dislocation density [5,14,28,30]. Moreover, as for conventional metal matrix micro-composites, the load transfer from the soft matrix to the hard particles under an applied load contributes to the strengthening of the base material. The volume fraction and aspect ratio of nanoparticles in MMnCs are generally quite low,

[1] For interpretation of color in 'Fig. 5', the reader is referred to the web version of this article.

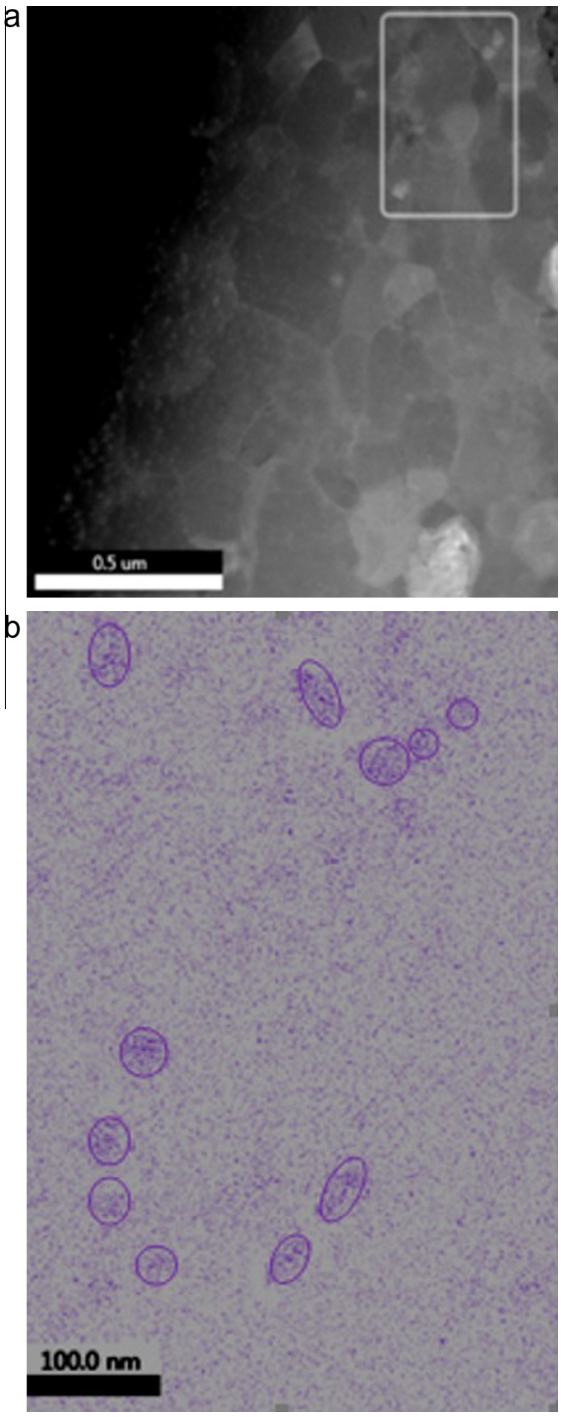

Fig. 6. (a) HAADF image of Al with in-situ Al_2O_3 NPs and (b) oxygen map of the area selected by the frame in (a).

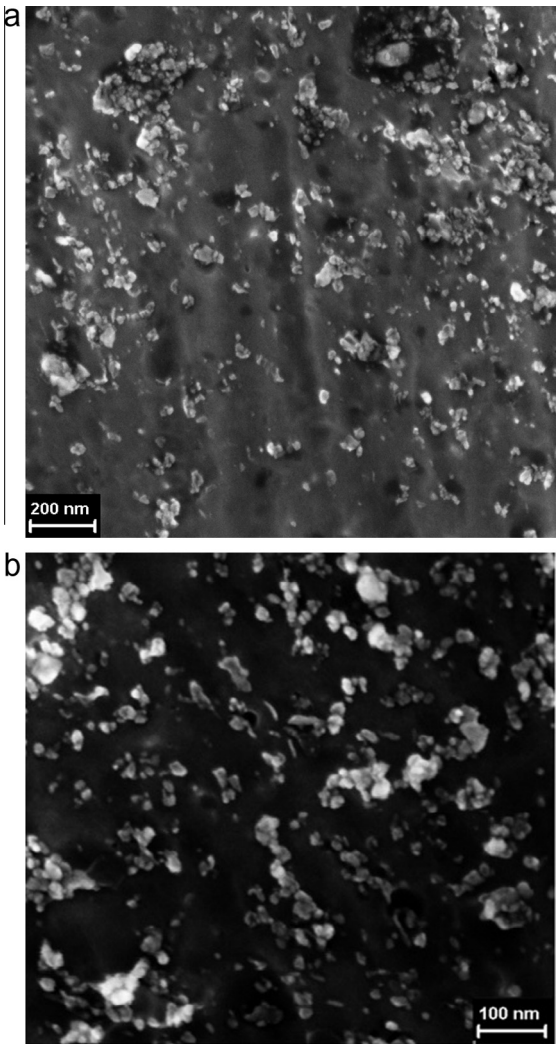

Fig. 7. SEM micrographs of Al with in-situ Al_2O_3 NPs as well as 2 wt.% ex-situ Al_2O_3 NPs at (a) low and (b) high magnifications.

and therefore the contribution from load transfer is considered relatively small [5]. The grain size has a strong influence on strength since the grain boundaries can obstruct dislocation movement. This is due to the different orientations of adjacent grains and to the high lattice disorder characteristic of the boundary regions, which prevent the dislocations from moving in a continuous slip plane [14]. The particles play an important role in the final grain size of the composites since they can hinder grain growth, acting as pinning points for grain boundary migration. According to the Zener equation [5], an increase in the volume fraction and a decrease in particle size lead to a finer grain structure. The Orowan mechanism relies on the interaction of nano-particles with dislocations. The nano-particles act as pinning points hampering the movement of the linear lattice defects and leading to dislocations bowing around the particles [27]. Also, the mismatch in CTE between the reinforcement and the metal matrix is believed to contribute to the final strength of nanocomposites. The aforementioned mismatch leads to the formation of dislocations, which are geometrically necessary to accommodate the different shrinking behaviors of the metal and the particles [30].

3.3. Mechanical spectroscopy

In Fig. 11, the results of damping tests are depicted in terms of $\tan\delta$ as a function of temperature. At 0.1, 1 or 10 Hz, a peak $\tan\delta$ is observed for both types of MMnCs. Higher amount of Al_2O_3 NPs led to better damping performance (i.e. higher $\tan\delta$) at temperatures higher than 50 °C for 0.1 Hz, 70 °C for 1 Hz and 100 °C for 10 Hz. The $\tan\delta$ (1 Hz) value for the monolithic CP aluminum is ~0.001 at 25 °C and ~0.007 at 275 °C [31]. Thus, a significant increase in internal friction was achieved in both MMnCs investigated. The damping behavior is strongly sensitive to lattice defects (point defects, dislocations, grain boundaries and interfaces) [26]. From Fig. 11, the shift of peaks towards higher temperatures can be clearly identified for both materials when the loading frequency

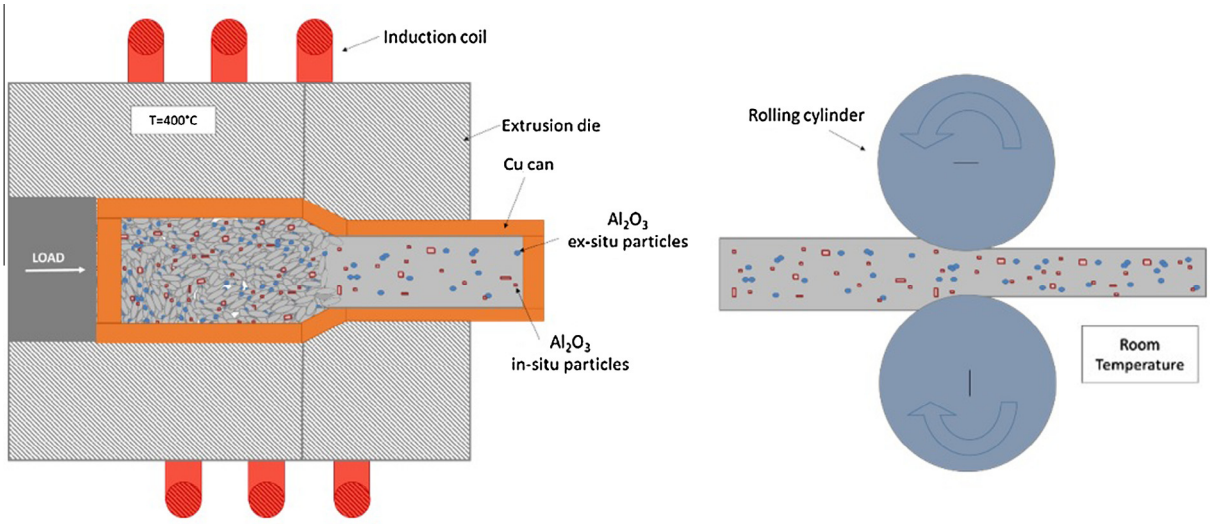

Fig. 8. Schematics of the hot extrusion consolidation and the cold rolling processes.

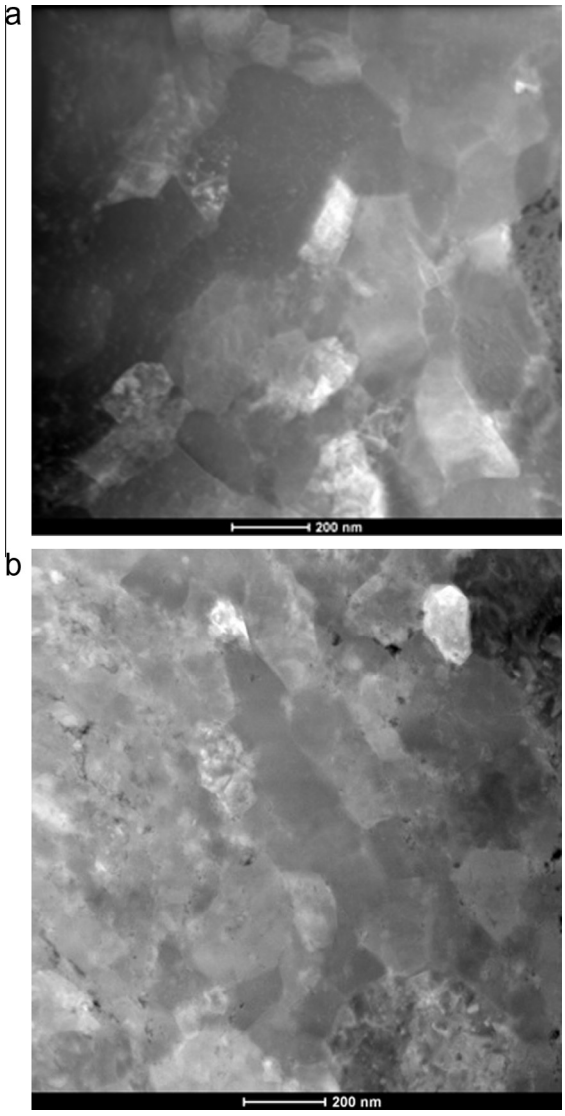

Fig. 9. HAADF images of (a) Al wire reinforced with in-situ Al_2O_3 NPs and (b) Al wire reinforced with in-situ Al2O3 NPs as well as 2 wt.% ex-situ Al_2O_3 NPs.

Table 2
Results of tensile tests on the MMnC wires and other pure Al.

	YS (MPa)	UTS (MPa)
Al wire + in-situ Al_2O_3 particles	225	302
Al wire + in-situ Al_2O_3 particles + 2 wt.% ex-situ Al_2O_3	282	373
Pure bulk Al [21]	~20	~30
Pure UFG bulk Al [21]	~110	~120

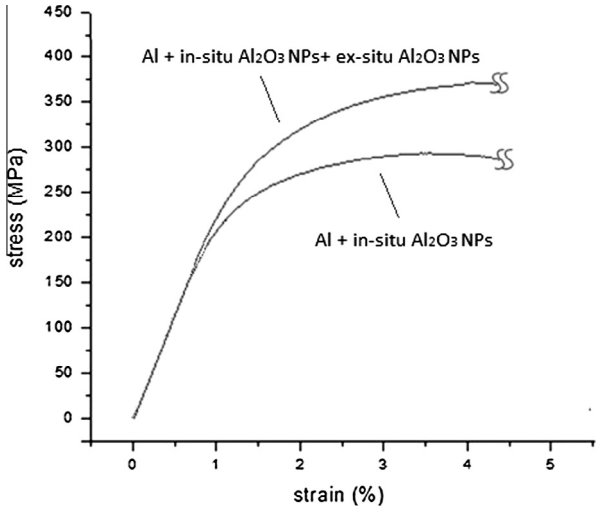

Fig. 10. Tensile stress–strain curves for the Al wire reinforced with Al_2O_3 NPs formed in-situ and the Al wire reinforced with both Al_2O_3 NPs formed in-situ and Al_2O_3 NPs added ex-situ.

is increased. This phenomenon is generally related to relaxation processes (relaxation type peak) [16,26,32]. The higher density of defects (higher micro-strain) and higher amount of interfaces in the wire reinforced with ex-situ Al_2O_3 are thought to cause the increased IF at high temperatures.

In fact, although the external applied stress is small, the internal stress concentration in regions of high dislocation density may be large enough to cause relative atomic sliding. At room temperature, the displacements are typically fractions of an atomic diameter whereas, at high temperatures, sliding can be much more

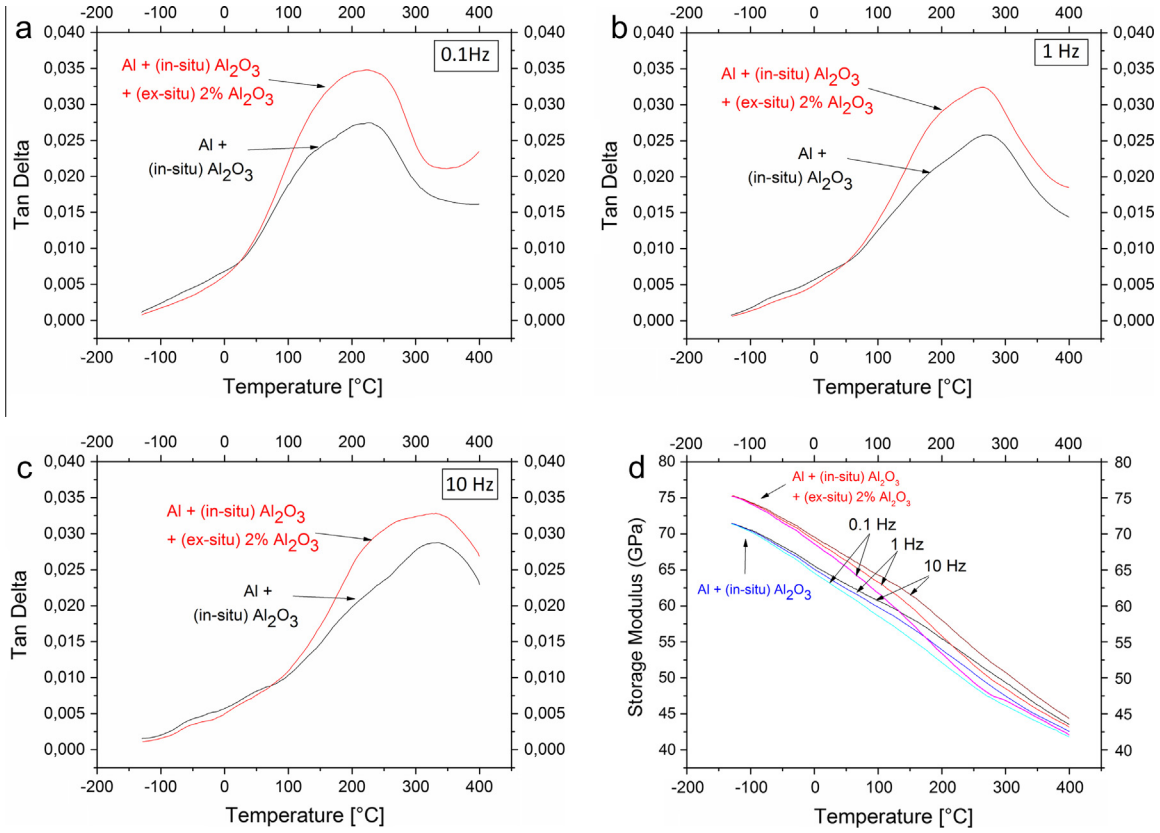

Fig. 11. Tan δ vs. temperature curves at (a) 0.1 Hz, (b) 1 Hz and (c) 10 Hz. (d) Storage modulus vs. temperature curves.

extensive and lead to viscoelastic strain. For this reason, the damping effects are more pronounced at elevated temperatures. However, with continued increase in temperature, dislocation mobility keeps increasing, resulting in annihilation of dislocations and eventually a decrease in tan δ [16,26,32]. The results show that the storage modulus of the MMnC reinforced with ex-situ NPs is higher than that of the MMnC reinforced only with in-situ NPs in the whole temperature range and for all the frequencies investigated (Fig. 11d), although as temperature increases the difference in the storage modulus decreases. This behavior can be related to the relaxation phenomena as well. At room temperature the storage modulus values reached by the in-situ and the ex-situ MMnCs are about 64 GPa and 68 GPa, respectively. The higher modulus of the composites is believed to be due to the combination of the elastic moduli of alumina and aluminum.

4. Conclusions

Al based nanocomposite wires were successfully produced via a powder metallurgy route based on high-energy ball milling, powder consolidation by hot extrusion and cold rolling. Ball milling led to fragmentation of the surface oxide layers on Al particles and the breakup of alumina clusters added ex-situ into nano-sized alumina particles. It was also able to homogeneously embed these nanoparticles in the Al matrix, producing the optimal precursors for subsequent consolidation. The milled powders were successfully consolidated by hot extrusion and then formed into wires by cold rolling without fracture. The process led to fully dense MMnCs characterized by well dispersed NPs and ultra-fine grains. The MMnCs so prepared showed excellent mechanical properties, especially compared to those of CP Al produced by conventional processes. The Al wire reinforced with ex-situ particles showed higher hardness, YS and UTS than the Al only reinforced with in-situ particles. Internal friction in the nanocomposites was determined at 0.1, 1 and 10 Hz, with well defined tan δ peaks. Higher amount of Al_2O_3 NPs leads to higher damping. The relaxation peak shifts towards higher temperatures with increasing loading frequency. The storage modulus of the MMnC reinforced with ex-situ NPs is higher than that of the MMnC reinforced with only in-situ NPs under the testing conditions.

References

[1] Tjong SC. Novel nanoparticle-reinforced metal matrix composites with enhanced mechanical properties. Adv Eng Mater 2007;9:639–52.
[2] Bakshi SR, Lahiri D, Agarwal A. Carbon nanotube reinforced metal matrix composites – a review. Int Mater Rev 2010;55:41–64.
[3] Casati R, Vedani M. Metal matrix composites reinforced by nano-particles – a review. Metals 2014;4(1):65–83.
[4] Arsenault RJ, Shi N. Dislocation generation due to differences between the coefficients of thermal expansion. Mater Sci Eng 1986;81:175–87.
[5] Casati R, Amadio M, Biffi CA, Dellasega D, Tuissi A, Vedani M. Al/Al_2O_3 nanocomposite produced by ECAP. Mater Sci Forum 2013;762:457–64.
[6] Casati R, Vedani M, Tuissi A, Villa E, Dellasega D, Wei X, et al. Microstructure and damping properties of ultrafined grained Al wires reinforced by Al_2O_3 nanoparticles. In: Grandfield John, editor. Light metals. California (USA): San Diego; 2014. p. 1347–51.
[7] Casati R, Ge Q, Vedani M, Dellasega D, Bassani P, Tuissi A. Sintering of pure aluminum and nano-alumina powders by ECAP and hot extrusion. Met Ital 2013;4:25–30.
[8] Balog M, Poletti C, Simancik F, Walcher M, Rajner W. The effect of native Al_2O_3 skin disruption on properties of fine Al powder compacts. J Alloy Compd 2011;509:S235–8.
[9] El-Kady Omyma, Fathy A. Effect of SiC particle size on the physical and mechanical properties of extruded Al matrix nanocomposites. Mater Des 2014;54:348–53.
[10] Jeyasimman D, Sivasankaran S, Sivaprasad K, Narayanasamy R, Kambali RS. An investigation of the synthesis, consolidation and mechanical behaviour of Al 6061 nanocomposites reinforced by TiC via mechanical alloying. Mater Des 2014;57:394–404.

[11] Li X, Yang Y, Cheng X. Ultrasonic-assisted fabrication of metal matrix nanocomposites. J Mater Sci 2004;39:3211–2.
[12] Liu Z, Han Q, Li J. Ultrasound assisted in situ technique for the synthesis of particulate reinforcedaluminum matrix composites. Composites B 2011;42:2080–4.
[13] Gupta M, Lai MO, Saravanaranganathan D. Synthesis, microstructure and properties characterization of disintegrated melt deposited Mg/SiC composites. J Mater Sci 2000;35:2155–65.
[14] Sanaty-Zadeh A, Rohatgi PK. Comparison between current models for the strength of particulate-reinforced metal matrix nanocomposites with emphasis on consideration of Hall–Petch effect. Mater Sci Eng A 2012;531:112–8.
[15] Huang Yi, Langdon Terence G. Advances in ultrafine-grained materials. Mater Today 2013;16:85–93.
[16] Zhang J, Perez RJ, Wong CR, Lavernia EJ. Effect of secondary phases on the damping behavior of metals, alloys and metal matrix composites. Mater Sci Eng R 1994;13:325–90.
[17] Lu H, Wang X, Zhang T, Cheng Z, Fang Q. Design, fabrication, and properties of high damping metal matrix composites—a review. Materials 2009;2: 958–77.
[18] Trunoc MA, Schoenitz M, Zhu X, Dreizin EL. Effect of polymorphic phase transformations in Al_2O_3 film on oxidation kinetics of aluminum powders. Combust Flame 2005;140:310–8.
[19] Phung X, Groza J, Stach EA, Williams LN, Ritchey SB. Surface characterization of metal nanoparticles. Mater Sci Eng, A 2003;359:261–8.
[20] Balog M, Simancik F, Walcher M, Rajner W, Poletti C. Extruded Al–Al_2O_3 composites formed in situ during consolidation of ultrafine Al powders: effect of the powder surface area. Mater Sci Eng, A 2011;529:131–7.
[21] Wafers K, Misra C. Oxides and hydroxides of aluminum. Alcoa Technical Report No. 19 Revised, Alcoa Laboratories; 1987. p. 64.
[22] Rufino B, Boulc'h F, Coulet M-V, Lacroix G, Denoyel R. Influence of particles size on thermal properties of aluminium powder. Acta Mater 2007;55:2815–27.
[23] Balog M, Krizik P, Nosko M, Hajovska Z, Castro Riglos MV, Rajner W, et al. Forged HITEMAL: Al-based MMCs strengthen with nanometric thick Al_2O_3 skeleton. Mater Sci Eng A 2014;613:82–90.
[24] Ge Q, Vedani M, Vimercati G. Extrusion of magnesium tubes for biodegradable stent precursors. Mater Manuf Processes 2012;27(2):140–6.
[25] Williamson, Hall. X-ray line broadening from filed aluminium and wolfram. Acta Metall 1953;1(1):22–31.
[26] Blanter MS, Golovin IS, Neuhauser H, Sinning H-R. Internal friction in metallic materials. Berlin Heidelberg: Springer Verlag; 2007.
[27] Zhan Z, Chen DL. Contribution of Orowan strengthening effect in particulate-reinforced metal matrix nanocomposites. Mater Sci Eng A 2008;483–484:148–52.
[28] Saravanan M, Pillai RM, Pai BC, Brahmakumar M, Ravi KR. Equal channel angular pressing of pure aluminium—an analysis. Bull Mater Sci 2006;29(7):679–84.
[29] Aluminium Alloys – New Trends in Fabrication and Applications, book edited by Zaki Ahmad, ISBN 978-953-51-0861-0, Published: December 5, 2012 under CC BY 3.0 license Chapter 1Equal-Channel Angular Pressing and Creep in Ultrafine-Grained Aluminium and Its Alloys By Vaclav Sklenicka, Jiri Dvorak, Milan Svoboda, Petr Kral and Marie Kvapilova.
[30] Koppad Praveennath G, AniruddhRam HR, Kashyap KT. On shear-lag and thermal mismatch model in multiwalled carbon nanotube/copper matrix nanocomposites. JALCOM 2013;549:82–7.
[31] Wei JN, Gong CL, Cheng HF, Zhou ZC, Li ZB, Shui JP, et al. Mater Sci Eng A 2002;332:375–81.
[32] Carreño-Morelli E, Urreta SE, Schaller R. Mechanical spectroscopy of thermal stress relaxation at metal–ceramic interfaces in Aluminium-based composites. Acta Mater 2000;48:4725–33.